

1 **Morphologic and Morphometric Differences between Gullies Formed** 2 **in Different Substrates on Mars: New Insights into the Gully** 3 **Formation Processes**

4 Rishitosh K. Sinha^{1,2}, Dwijesh Ray¹, Tjalling De Haas³, Susan J. Conway⁴, Axel Noblet⁴

5 ¹ Physical Research Laboratory, Ahmedabad 380009, Gujarat, India

6 ² Indian Institute of Technology, Gandhinagar 382355, Gujarat, India

7 ³ Faculty of Geoscience, Universiteit Utrecht, Princetonlaan 8a, 3584 CB Utrecht, the Netherlands

8 ⁴ Nantes Université, Université d'Angers, Le Mans Université, CNRS UMR 6112 Laboratoire de Planétologie et Géosciences,
9 France

10

11 *Correspondence to:* Rishitosh K. Sinha (rishitosh@prl.res.in)

12 **Abstract.** Martian gullies are kilometer-scale geologically young features with a source alcove, transportation channel, and
13 depositional fan. On the walls of impact craters, these gullies typically incise into bedrock or surfaces modified by latitude
14 dependent mantle (LDM; inferred as consisting ice and admixed dust) and glaciation. To better understand the differences in
15 alcoves and fans of gullies formed in different substrates and infer the flow types that led to their formation, we have analyzed
16 the morphology and morphometry of 167 gully systems in 29 craters distributed between 30°S and 75°S. Specifically we
17 measured length, width, gradient, area, relief, and relief ratio of alcove and fan, Melton ratio, relative concavity index, and
18 perimeter, form factor, elongation ratio and circularity ratio of the alcoves. Our study reveals that alcoves formed in
19 LDM/glacial deposits are more elongated than the alcoves formed in bedrock, and possess a distinctive V-shaped cross section.
20 We have found that mean gradient of fans formed by gullies sourced in bedrock is steeper than the mean gradient of fans of
21 gullies sourced in LDM/glacial deposits. These differences between gullies were found to be statistically significant and
22 discriminant analysis has confirmed that alcove perimeter, alcove relief and fan gradient are the most important variables for
23 differentiating gullies according to their source substrates. The comparison between the Melton ratio, alcove length and fan
24 gradient of Martian and terrestrial gullies reveals that Martian gully systems were likely formed by terrestrial debris-flow like
25 processes. It is likely that the present-day sublimation of CO₂ ice on Mars provided the adequate flow fluidization for the
26 formation of deposits akin to terrestrial debris-flow like deposits.

27 **1 Introduction**

28 Gullies are found on steep slopes polewards of about 30° latitude in both hemispheres on Mars and manifest as kilometer-
29 scale, geologically young features (formed within the last few million years) comprising an alcove, channel, and depositional
30 fan (Malin and Edgett, 2000; Dickson et al., 2007; Reiss et al., 2004; Schon et al., 2009). Gullies occur in a wide assortment

31 of settings, varying from the walls and central peaks of craters to walls of valleys, and steep faces of dunes, hills and polar pits
32 (e.g. Balme et al., 2006; Dickson et al., 2007; Dickson and Head, 2009; Conway et al., 2011, 2015; Harrison et al., 2015). On
33 the walls of craters, gullies are found to have incised into the (1) surfaces covered by latitude dependent mantle (LDM; e.g.
34 Mustard et al., 2001; Dickson et al., 2012, 2015), (2) surfaces modified by former episodes of glaciation (Hubbard et al., 2011;
35 Souness et al., 2012; Souness and Hubbard, 2012; Sinha and Vijayan, 2017), and (3) bedrock (e.g. Johnsson et al., 2014; de
36 Haas et al., 2019a; Sinha et al., 2020). Detailed investigation of the gullies formed over these different substrates is key to
37 understanding the intricacies of past processes by which these gullies have formed on Mars (Conway et al., 2015; de Haas et
38 al., 2019a).

39 A variety of models have been proposed to explain the formation of gullies, which include: (1) dry flows triggered by
40 sublimation of CO₂ frost (e.g. Cedillo-Flores et al., 2011; Dundas et al., 2012, 2015; Pilorget and Forget, 2016; de Haas et al.,
41 2019b), (2) debris-flows of an aqueous nature (e.g. Costard et al., 2002; Levy et al., 2010; Conway et al., 2011; Johnsson et
42 al., 2014; de Haas et al., 2019a; Sinha et al., 2020), and (3) fluvial flows (e.g. Heldmann and Mellon, 2004; Heldmann et al.,
43 2005; Dickson et al., 2007; Reiss et al., 2011). To better understand the gully formation processes, morphometric investigation
44 of gullies formed over different substrates needs to be undertaken at a level of detail previously not attempted.

45 The global distribution of gullies shows a spatial correlation with the landforms indicative of glaciation and LDM deposition
46 on Mars (e.g. Levy et al., 2011; Dickson et al., 2015; Harrison et al., 2015; Conway et al., 2018; de Haas et al., 2019a; Sinha
47 et al., 2020). With respect to glacial landforms, many gullies have formed into viscous flow features (VFF) and they are found
48 in the same extent of latitudes (e.g. Arfstrom and Hartmann, 2005; de Haas et al., 2018). VFFs are defined as an umbrella term
49 for glacial-type formations covering a broad range of landforms that include lobate debris aprons, concentric crater fill, and
50 lineated valley fills (e.g. Squyres, 1978; Levy et al., 2009; Baker et al., 2010; Hargitai, 2014). Together, they are inferred to
51 be similar to terrestrial debris-covered glaciers (Conway et al., 2018). With respect to LDM, gullies are mostly found on the
52 pole-facing slopes of crater walls at lower mid-latitudes (30-45°) (e.g. Balme et al. 2006; Kneissl et al. 2010; Harrison et al.
53 2015; Conway et al. 2017), wherein, LDM is found to be dissected (e.g. Mustard et al., 2001; Milliken et al., 2003; Head et
54 al., 2003). In the higher latitudes (>45°), LDM is found to be continuous (e.g. Kreslavsky and Head, 2000), and gullies are
55 evident at both the pole and equator facing slopes (e.g. Balme et al. 2006; Kneissl et al. 2010; Harrison et al. 2015; Conway et
56 al. 2017). Gullies formed on the formerly glaciated walls of craters are fed from alcoves that do not extend up to the crater rim,
57 and appear elongated to V-shaped, implying gully-channel incision into ice-rich, unlithified sediments (e.g. Aston et al., 2011;
58 de Haas et al., 2019a). The alcoves, channels and fan deposits of gullies formed within craters covered by a smooth drape of
59 LDM, are usually found to have experienced multiple episodes of LDM covering and subsequent reactivation of some of the
60 pre-existing channels or formation of fresh channels within the draped LDM deposits (e.g. Dickson et al., 2015; de Haas et al.,
61 2019a). Additionally, there are gullies that directly emanate from well-defined bedrock alcoves that cut into the crater rim in
62 the absence of LDM and/or glacial deposits (e.g. Johnsson et al., 2014; de Haas et al., 2019a; Sinha et al., 2020). Gullies

63 formed in these craters have alcoves with sharply defined crests and spurs, exposing the underlying bedrock, and meter-sized
64 boulders are found throughout the gully system (e.g. Johnsson et al., 2014; de Haas et al., 2019a; Sinha et al., 2020). Further,
65 De Haas et al., 2015a found that the stratigraphy of the fans whose source area was in bedrock were more boulder-rich than
66 those fans fed by catchments in LDM. The findings in these studies suggest that a more detailed investigation of the
67 morphology and morphometry of the gullies formed over contrasting substrates is important for improving our understanding
68 of the formative mechanisms of gullies.

69 In this work, we focus on addressing the following research questions:

70 (1) Do the morphology and morphometry of gully systems formed in different substrates differ (i.e. LDM/glacial deposits and
71 bedrock)?

72 (2) How do the morphometric characteristics of gullies formed on Mars compare to those formed by a range of processes on
73 Earth, and what does that tell us about the formative processes of Martian gullies?

74 To parameterize the morphometry we will primarily study long profiles. Previously, only a few studies have analyzed the
75 morphometric characteristics of the gullies by studying long profiles of gullies (e.g. Yue et al., 2014; Conway et al., 2015; De
76 Haas et al., 2015a; Hobbs et al., 2015). These studies have focused observations on a part of the gully system and suggested
77 that the differences in the properties of substrate into which the gullies incise play a significant role in promoting the flows
78 that led to gully formation. Hence, for a more detailed differentiation of the gully types and interpretation of the dominant flow
79 type that led to gully formation on Mars, quantification of the morphometric characteristics of the entire gully system is crucial.

80 **2 Study sites and datasets**

81 We characterize the morphology and morphometry of gullies in 29 craters distributed over the southern hemisphere between
82 30° S and 75° S latitude (Fig. 1). These 29 craters are selected based on the availability of publicly released High Resolution
83 Imaging Science Experiment (HiRISE) stereo-pair based digital terrain model (DTM) or the presence of suitable HiRISE
84 stereo-pair images to produce a DTM ourselves. The HiRISE stereo-pair images are usually ~0.25 - 0.5 m/pixel (McEwen et
85 al., 2007), so the DTM post spacing is ~1-2 m with vertical precision in the range of tens of centimeters (Kirk et al., 2008).
86 Among the 29 gullied craters, publicly released DTMs are available for 25 craters
87 (<https://www.uahirise.org/hiwish/maps/dtms.jsp> - last accessed 18th September 2021) (Table 1). For the remaining 4 craters,
88 DTMs are produced with the software packages USGS ISIS and BAE Systems SocetSet (Table 1) (Kirk et al., 2008). We
89 investigated HiRISE images of these 29 gullied craters for detailed morphological characterization of the substrate into which
90 the crater wall gullies incise (Table 1).

91

92

93 **Table 1.** Summary of the craters included in this study, their locations, number of gullies investigated from the crater, substrate
 94 on the crater wall in which gullies have incised, key morphological attributes of the substrate, and IDs of HiRISE imagery and
 95 DTM used for morphological and morphometric investigation of gullies in these craters.

Crater	Latitude	Longitude	No. of gullies	Substrate	Key morphological attributes	HiRISE ID	HiRISE DTM ID
Artik	34.8° S	131.02° E	2	LDM/glacial deposits	Polygons, V-shaped incisions, arcuate ridges, small-scale lobate debris aprons (LDAs) on the floor	ESP_020740_1450	DTEEC_012459_1450_012314_1450_A01
Asimov	47.53° S	4.41° E	4	LDM/glacial deposits	Polygons, V-shaped incisions, mantled alcoves/channels/fans, arcuate ridges, small-scale LDAs inside valleys	ESP_012912_1320	DTEEC_012912_1320_012767_1320_A01
Bunnik	38.07° S	142.07° W	8	LDM/glacial deposits	Polygons, V-shaped incisions, mantled alcoves/channels/fans, arcuate ridges	ESP_047044_1420	DTEEC_002659_1420_002514_1420_U01
Corozal	38.78° S	159.48° E	6	LDM/glacial deposits	Polygons, mantled alcoves/channels/fans, arcuate ridges, small-scale LDAs on the floor	PSP_006261_1410	DTEEC_006261_1410_014093_1410_A01
Dechu	42.23° S	158° W	8	LDM/glacial deposits	Polygons, mantled alcoves/channels/fans, arcuate ridges, small-scale LDAs on the floor	PSP_006866_1375	DTEED_023546_1375_023612_1375_A01
Dunkassa	37.46° S	137.06° W	5	LDM/glacial deposits	Polygons, V-shaped incisions, mantled alcoves/channels/fans, arcuate ridges, small-scale LDAs on the floor	ESP_032011_1425	DTEEC_039488_1420_039343_1420_A01
Hale	35.7° S	36.4° W	8	LDM/glacial deposits	Polygons, V-shaped incisions, mantled alcoves/channels/fans, talus slope deposits	PSP_003209_1445	DTEEC_002932_1445_003209_1445_A01
Langtang	38.13° S	135.95° W	5	LDM/glacial deposits	Polygons, V-shaped incisions, mantled alcoves/channels/fans, arcuate ridges, small-scale LDAs on the floor	ESP_030099_1415	DTEEC_024099_1415_023809_1415_U01

Moni	46.97° S	18.79° E	5	LDM/glacial deposits	Partly infilled alcoves, mantled fan surfaces, arcuate ridges	ESP_056862_1325	DTEEC_007110_1325_006820_1325_A01
Nybyen	37.03° S	16.66° W	8	LDM/glacial deposits	Polygons, mantled alcoves/channels/fans, arcuate ridges	ESP_059448_1425	DTEEC_006663_1425_011436_1425_A01
Palikir	41.56° S	157.87° W	5	LDM/glacial deposits	Polygons, V-shaped incisions, mantled alcoves/channels/fans, arcuate ridges, small-scale LDAs on the floor	ESP_057462_1380	DTEEC_005943_1380_011428_1380_A01
Penticton	38.38° S	96.8° E	7	LDM/glacial deposits	Polygons, V-shaped incisions, mantled alcoves/channels/fans, arcuate ridges, small-scale LDAs on the floor	ESP_029062_1415	DTEEC_001714_1415_001846_1415_U01
Selevac	37.37° S	131.07° W	8	LDM/glacial deposits	Polygons, mantled alcoves/channels/fans, small-scale flows on the floor	ESP_045158_1425	DTEEC_003252_1425_003674_1425_A01
Raga	48.1° S	117.57° W	4	LDM	Polygons, mantled alcoves/channels/fans	ESP_041017_1315	DTEEC_014011_1315_014288_1315_A01
Roseau	41.7° S	150.6° E	1	LDM	Polygons, mantled alcoves/channels/fans	ESP_024115_1380 / ESP_011509_1380	ESP_024115_1380_ESP_011509_1380*
Taltal	39.5° S	125.8° W	7	LDM/glacial deposits	Polygons, V-shaped incisions, mantled alcoves/channels/fans, arcuate ridges, small-scale LDAs on the floor	ESP_037074_1400 / ESP_031259_1400	ESP_037074_1400_ESP_031259_1400*
Talu	40.34° S	20.11° E	7	LDM/glacial deposits	Polygons, V-shaped incisions, mantled alcoves/channels/fans, arcuate ridges, small-scale LDAs on the floor	ESP_011817_1395	DTEEC_011817_1395_011672_1395_O01
Triolet	37.08° S	168.02° W	4	LDM/glacial deposits	Polygons, V-shaped incisions, mantled alcoves/channels/fans, arcuate ridges, small-scale LDAs on the floor	ESP_047190_1425	DTEEC_023586_1425_024008_1425_A01
Unnamed crater	32.31° S	118.55° E	4	LDM/glacial deposits	Polygons, mantled alcoves/channels/fan	PSP_006869_1475	DTEEC_021914_1475_022336_1475_U01

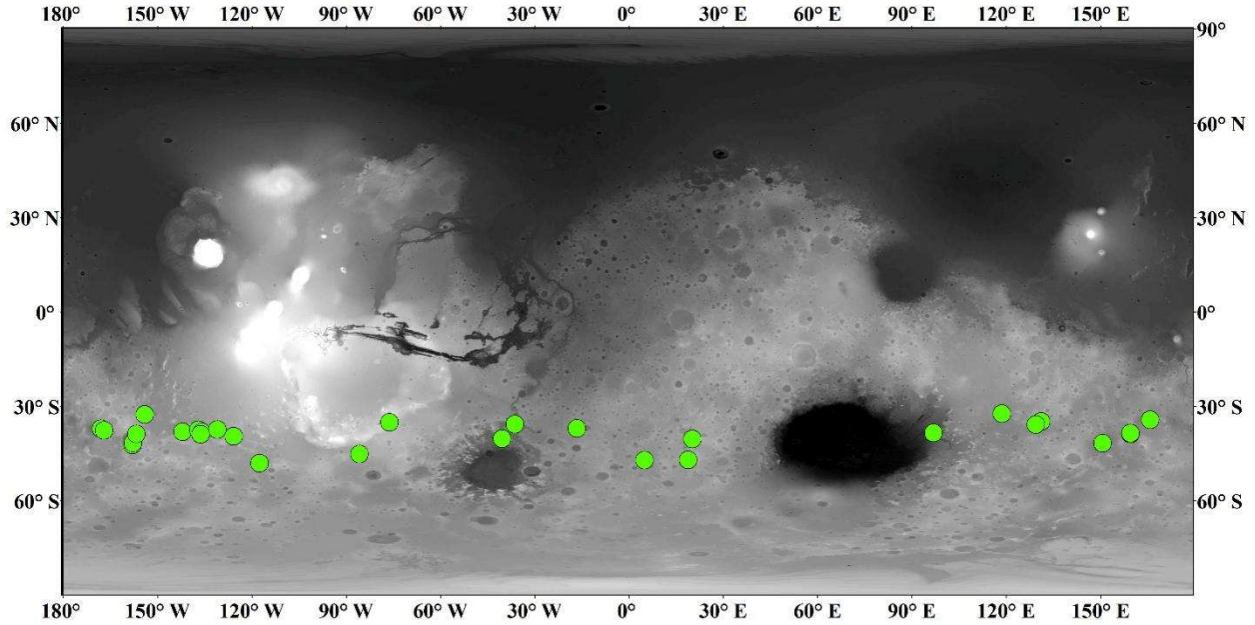
					s, arcuate ridges, small-scale LDAs on the floor		
Unnamed crater in the Argyre basin	40.3° S	40.4° W	6	LDM/glacial deposits	Polygons, mantled alcoves/channels/fans, arcuate ridges, small-scale LDAs on the floor	ESP_032047_1395	DTEEC_012795_1395_013507_1395_A01
Unnamed crater in the Newton basin	38.8° S	156.8° W	5	LDM	Polygons, V-shaped incisions, mantled alcoves/channels/fans	PSP_002686_1410	DTEEC_002620_1410_002686_1410_A01
Unnamed crater north of Corozal crater	38.53° S	159.44° E	5	LDM/glacial deposits	Polygons, mantled alcoves/channels/fans, small-scale LDAs on the floor	ESP_020884_1410	DTEEC_020884_1410_020950_1410_A01
Unnamed crater-1 in the Terra Sirenum	32.55° S	154.11° W	2	LDM	Mantled alcoves/channels/fans	PSP_007380_1470	DTEEC_010597_1470_007380_1470_U01
Unnamed crater-2 in the Terra Sirenum	38.88° S	136.36° W	6	LDM/glacial deposits	Polygons, V-shaped incisions, mantled alcoves/channels/fans, arcuate ridges, small-scale LDAs on the floor	ESP_020407_1410	DTEEC_022108_1410_022385_1410_A01
Istok	45.1° S	85.82° W	8	Bedrock	Alcove cut directly into the original crater-wall material, clasts embedded into fresh deposits on fan	ESP_056668_1345	DTEEC_040607_1345_040251_1345_A01
Galap	37.66° S	167.07° W	8	Bedrock	Alcove cut directly into the original crater-wall material, clasts embedded into fresh deposits on fan	ESP_059770_1420	DTEEC_048983_1420_048693_1420_U01
Gasa	35.73° S	129.4° E	7	Bedrock	Alcove cut directly into the original crater-wall material, clasts embedded into fresh deposits on fan	ESP_057491_1440	DTEEC_021584_1440_022217_1440_A01
Los	35.08° S	76.23° W	7	Bedrock	Alcove cut directly into the original crater-wall material,	ESP_020774_1445 / ESP_050127_1445	ESP_020774_1445_ESP_050127_1445*

					clasts embedded into fresh deposits on fan		
Unnamed crater-3 in the Terra Sirenum	34.27° S	165.71° E	7	Bedrock	Alcove cut directly into the original crater-wall material, clasts embedded into fresh deposits on fan	ESP_049261_1455 / ESP_049828_1455	ESP_049261_1455_ ESP_049828_1455*

96

97 (*) DTMs are produced with the software packages USGS ISIS and BAE Systems SocetSet.

98



99 Figure 1: Locations of craters analyzed in this study (green circles). Background: Mars Orbiter Laser Altimeter gridded data, where
 100 white is high elevation and black is low elevation, credit MOLA Science Team/NASA/JPL.

101

102 3 Approach

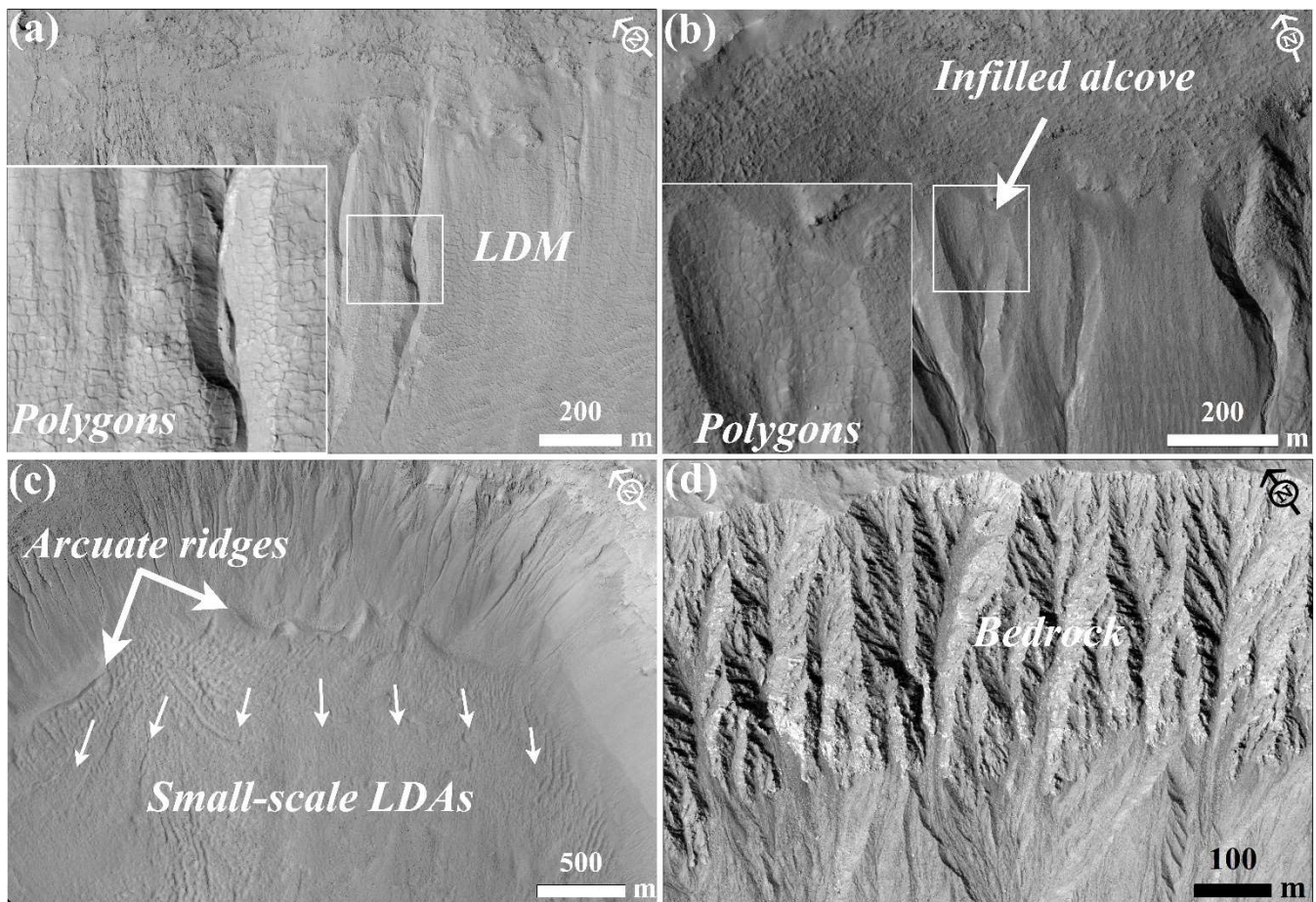
103 3.1 Identification of substrate

104 The substrate into which the gullies have incised is identified based on the following criteria:

- 105 1. LDM/glacial deposits: Any crater whose gullies incise walls that appear to be softened by the drape of smooth mantling
 106 material with polygonal cracks is inferred to have LDM as the substrate within which gullies have incised (e.g. Mustard et al.,

107 2001; Kreslavsky and Head, 2002; Levy et al., 2009a; Conway et al., 2018; de Haas et al., 2019a) (Fig. 2a). The alcoves on
108 the walls of these craters may be partially to completely filled by LDM, and in some cases, polygonized LDM materials may
109 be seen covering the alcove walls (e.g. Christensen, 2003; Conway et al., 2018; de Haas et al., 2019a). These infilled alcoves
110 on the crater walls are not the alcoves of gullies formed within the LDM substrate; instead, they represent the alcoves that were
111 formed prior to the LDM emplacement epoch. Additionally, gullied craters that show evidence in the form of arcuate ridges at
112 the foot of the walls and VFFs that cover part or the entire crater floor are inferred to have been modified by one or multiple
113 episodes of glaciation (e.g. Arfstrom and Hartmann, 2005; Head et al., 2010; Milliken et al., 2003; Hubbard et al., 2011). These
114 craters host gullies that are often partially or fully covered by LDM deposits.

115 2. Bedrock: Craters where the features listed in LDM/glacial deposits are absent and where rocky material is visible extending
116 downwards from the crater rim. This rocky material usually outcrops as spurs and can be layered or massive. The slopes can
117 be smooth or covered with boulders, with concentrations of boulders at the slope toe.



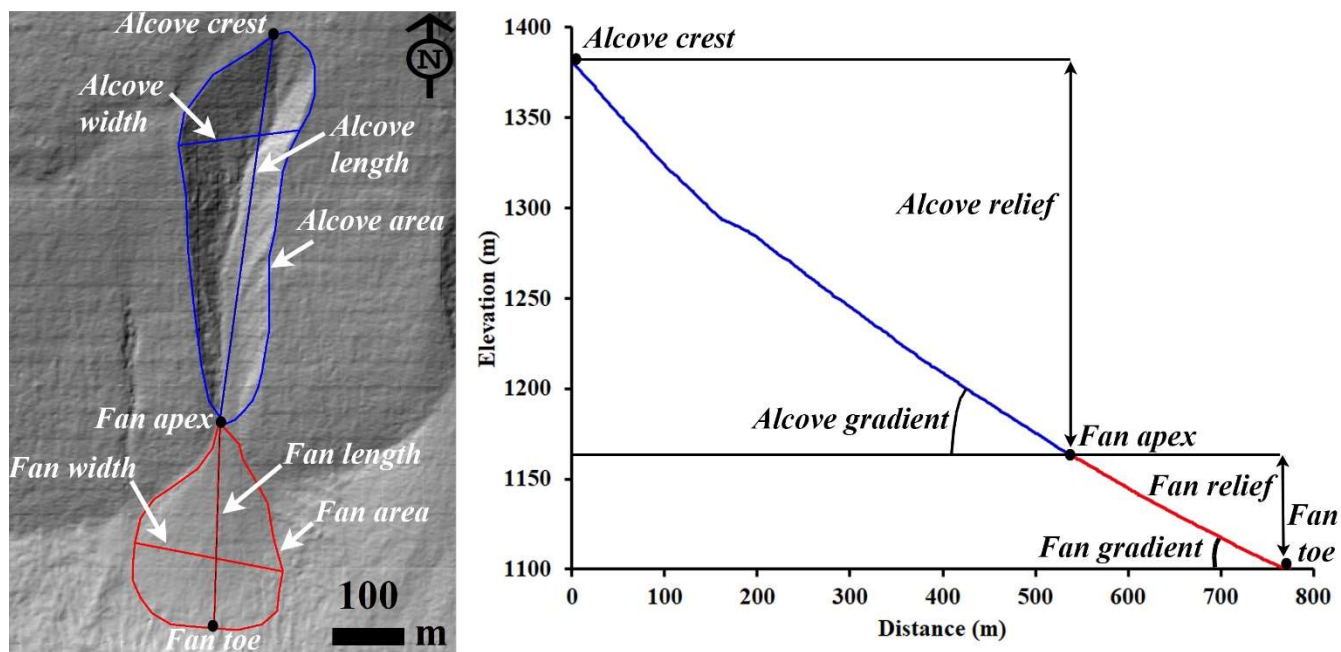
118

119 Figure 2: Examples of morphological evidence used to identify LDM, glacial deposits, and bedrock. (a) Smooth mantling material
 120 inferred as LDM draped on the wall of Talu crater on the basis of polygonal cracks formed in the material. The bigger box is an
 121 expanded view of the polygons seen over the region outlined by the smaller box. (HiRISE image ESP_011817_1395). (b) An infilled
 122 alcove on the wall of an unnamed crater-2 in the Terra Sirenum. Evidence of polygons in the infilled material suggests presence of
 123 LDM deposits draped on the wall. The region shown in smaller box is expanded in the bigger box to show evidence of the polygons.
 124 (HiRISE image ESP_020407_1410). (c) Glaciation inferred in the Corozal crater on the basis of arcuate ridges formed at the foot of
 125 the crater wall and small-scale LDAs on the crater floor. Arrows indicate the downslope flow of LDAs on the floor. (HiRISE image
 126 PSP_006261_1410). (d) Exposed fractured bedrock identified on the walls of Istok crater within which alcoves have incised. (HiRISE
 127 image ESP_056668_1345). HiRISE image credit: NASA/JPL /University of Arizona.

128

129 3.2 Morphometric variables

130 The measurements we made of each gully system include alcove area, alcove perimeter, alcove length, alcove width, alcove
 131 gradient, fan area, fan length, fan width, and fan gradient (Fig. 3). In total, we derived 18 morphometric variables to
 132 characterize each gully fan and its alcove. The morphometric variables are classified into geometry, relief, gradient, and
 133 dimensionless variables and they are calculated with established mathematical equations shown in Table 2. For the gradient
 134 measurement using the DTM, the topographic profile from (1) crest of the alcove to the apex of the fan was extracted for the
 135 alcove, and (2) apex to foot of the fan was extracted for the fan.



136

137 Figure 3: Examples of morphometric variables estimated in this work. Left panel: HiRISE DTM (Id:
 138 DTEEC_002659_1420_002514_1420) based hillshade. HiRISE DTM credit: NASA/JPL /University of Arizona. Right panel:

139 **Topographic profile: blue profile represents the topography of gully alcove from alcove top to fan apex and red profile represents**
 140 **the profile of gully fan from fan apex to fan toe.**

141

142

143 **Table 2.** Set of morphometric variables extracted from the studied gully systems and their formulas and/or description of
 144 method.

Morphometric variable	Formula and/or description of method	References
Alcove length and width	Measured in km	Tomczyk, 2021
Alcove area	Measured in km ²	Tomczyk, 2021
Fan length and width	Measured in km	Tomczyk, 2021
Fan area	Measured in km ²	Tomczyk, 2021
Melton ratio	(Alcove relief)/(Alcove area ^{-0.5})	Melton, 1957
Relative concavity index (RCI)	Concavity Index/(maximum relief between the uppermost and lowermost points along the gully fan profile/2). Concavity Index is estimated as $\sum (H_i^* - H_i) / N$, where H_i^* is the elevation along the straight line, H_i is the elevation along the gully fan profile, N is the total number of measurement points.	Langbein, 1964; Phillips and Lutz, 2008
Alcove gradient	Measured in (°)	Tomczyk, 2021
Fan gradient	Measured in (°)	Tomczyk, 2021
Alcove relief	Measured in km	Tomczyk, 2021
Fan relief	Measured in km	Tomczyk, 2021
Relief ratio (alcove and fan)	Alcove/fan relief divided by the length of the alcove/fan	Schumm, 1956a, b
Perimeter	Measured in km	Schumm, 1956a, b
Form factor	Alcove area divided by the square of the length of the alcove	Horton, 1932
Elongation ratio	Diameter of a circle of the same area as the alcove divided by the maximum alcove length	Schumm, 1956a, b
Circularity ratio	Alcove area divided by the area of the circle having the same perimeter as the alcove perimeter	Miller, 1953

145

146 **3.3 Gully system selection for morphometric measurements**

147 We have selected only those gully systems for morphometric measurements in which: (i) the depositional fan from an alcove-
 148 channel system is not superimposed by or interfingering with the fans from the neighboring channels, (ii) there is clear
 149 association between the primary channel emanating from the alcove that extends downslope and then deposit its respective
 150 fan, (iii) no evidence of extensive cross-cutting is seen with the neighboring channels on the walls, (iv) no evidence of extensive
 151 mantling by dust/aeolian deposits is apparent, and (v) no evidence of channel/fan superposition on any topographic obstacle
 152 on the walls or the floor of the crater is apparent, which may have influenced the morphometry. If in any case the fans

153 superimpose or channels cross-cut, we have carefully demarcated the alcove-channel-fan boundary, to minimize the
154 inaccuracies in the measurements. Note that the selection of the gully systems was also constrained by the coverage of HiRISE
155 DTM that was used for morphometric analysis.

156 **3.4 Statistical analysis of morphometric variables**

157 We have two groups of gullies in our study: (1) gullies whose source area is incised into LDM/glacial deposits and (2) gullies
158 whose source area is incised into the bedrock. First, for both the groups we have calculated descriptive statistics for each of
159 the morphometric variables shown in Table 2. The significance of the difference between the values of each of the
160 morphometric variables calculated for each group was tested using a Student's t-test. To apply t-tests, we have transformed
161 the morphometric variables to remove skewness by taking their natural logarithm. Correlation analysis has been used to
162 investigate the correlation between the selected morphometric attributes of alcoves and fans. We infer strong positive
163 correlations between variables if the correlation coefficient value is more than 0.7 and strong negative correlations if the value
164 is less than -0.7. Very strong positive correlation between variables is inferred if the correlation coefficient is ≥ 0.9 . Further,
165 we used canonical discriminant analysis (CDA) to determine morphometric variables that provide the most discrimination
166 between the groups of gullies. In CDA, functions are generated according to the number of groups, until a number equal to n-
167 1 functions is reached (n is the number of groups) (Conway et al., 2015). For the two groups of gullies in our study, there is
168 going to be a function for which there is a standardised canonical discriminant function coefficient associated with the
169 morphometric variable. The higher the magnitude of this coefficient for a particular morphometric variable, the higher the role
170 of that variable in separating the groups of gullies. Standardisation was done by dividing each value for a given variable by
171 the maximum value.

172 **4 Results**

173 **4.1 Morphology of gully systems**

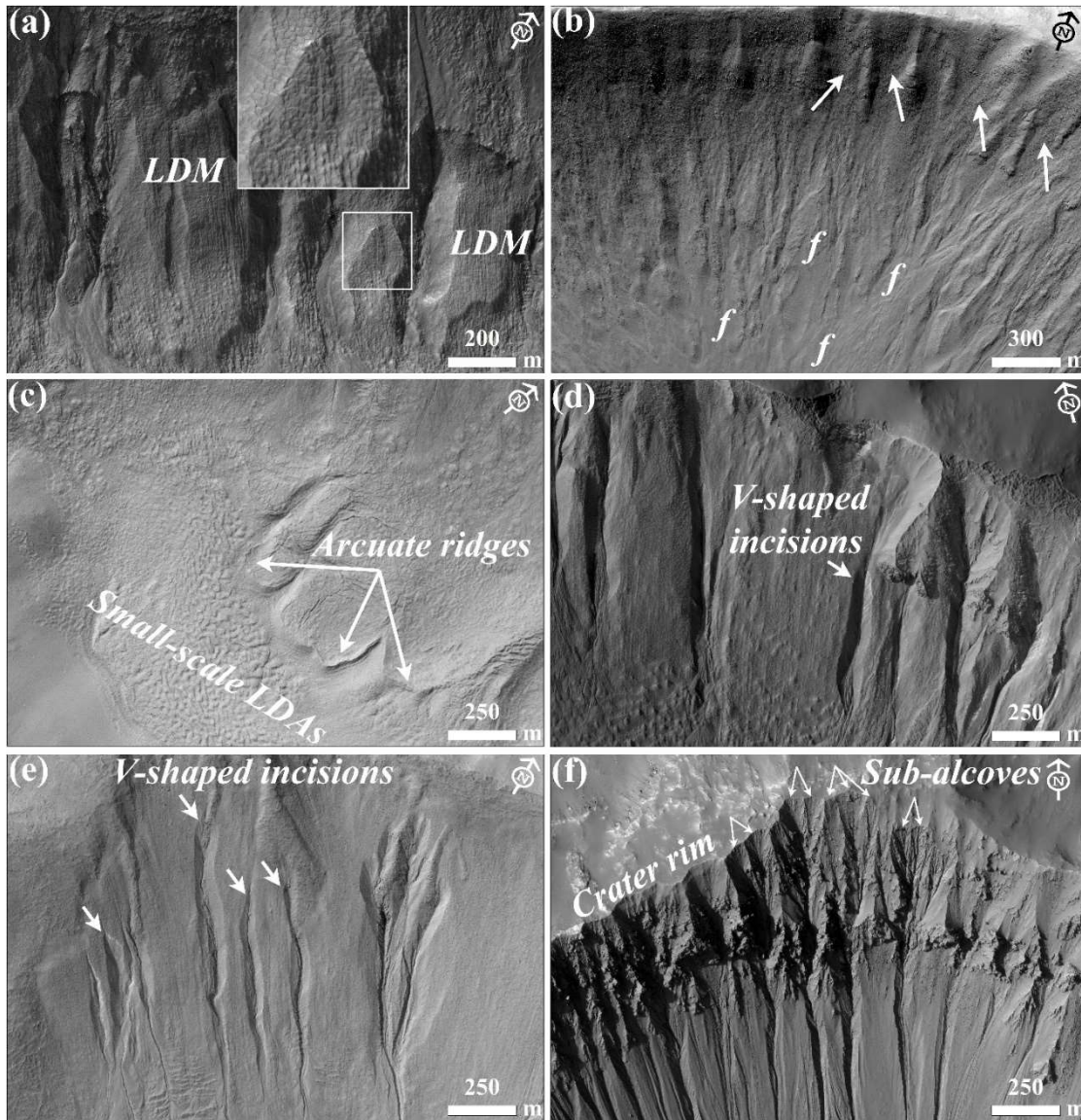
174 Out of the 29 gullied craters analysed in this work, we have found that there are 24 craters influenced by LDM and VFFs. The
175 remaining 5 craters have gullies incised into the exposed underlying bedrock on the wall of the crater. Below we describe the
176 substrates identified in the studied craters and then compare the morphology of the gullies formed into those substrates.

177 4 craters out of 24 craters (i.e. Raga, Roseau, unnamed crater in Newton basin and unnamed crater-1 in Terra Sirenum) have
178 gullies that are only influenced by LDM. In these craters, we have found morphological evidence of LDM in the form of
179 polygonized, smooth textured material on the pole-facing walls of the craters. Morphological evidence of VFF is not evident
180 in these craters. In these craters, the gully-alcoves and gully channels appear to have been incised into the polygonized LDM
181 material, and the gully-fan deposits are mantled. A typical example of this can be found in the unnamed crater formed inside
182 the Newton basin (Fig. 4a). Roseau crater, in particular, contains a large number of gully systems whose alcoves and fans are

183 extensively mantled (Fig. 4b). The remaining 20 out of 24 craters contain evidence for gullies that are influenced by both LDM
184 and glacial deposits (Table 1). The base of the pole-facing walls and the floor of the craters within which the gully systems
185 have formed host linear-to-sinuuous arcuate ridges and VFFs, respectively. Typical examples of VFFs can be found in Corozal,
186 Talu, unnamed craters in Terra Sirenum and Argyre basin, Langtang, Dechu and Dunkassa craters (Fig. 4c). In majority of the
187 gullied craters (except Raga, Roseau and unnamed crater-1 in Terra Sirenum) influenced by LDM and glacial deposits, gully
188 alcoves are found to have a distinctive V-shaped cross section in their mid-section (Figures 4d and 4e), they do not extend up

189 to the crater rim, and gully systems often show multiple episodes of activity, inferred by the presence of fresh channel incision
190 on the gully-fan surfaces (Fig. 4d-e).

191 Istok, Galap, Gasa, Los, and an unnamed crater in the Terra Sirenum contain gully systems on the pole-facing walls that are
192 not associated with LDM and VFFs (Table 1). The alcoves inside these craters have a crenulated shape and appear to have
193 formed by headward erosion into the bedrock of the crater rim (Fig. 4f). These craters have formed large gully systems on
194 their pole-facing walls, with brecciated alcoves, comprising of multiple sub-alcoves and hosting many clasts/boulders (Fig.
195 4f).



213 **Figure 4: (a) LDM draped on the wall of an unnamed crater in the Newton basin. The inset shows details of the polygonal texture of**
214 **the LDM. (HiRISE image PSP_002686_1410). (b) Infilled alcoves (arrows) and mantled fan surfaces (marked by letter ‘f’) on the**
215 **wall of Roseau crater. (HiRISE image ESP_024115_1380). (c) Arcuate ridges at the foot of the crater wall and small-scale LDAs on**
216 **the floor in Langtang crater. (HiRISE image ESP_030099_1415). (d) V-shaped incisions on the LDM draped walls of Taltal (HiRISE**
217 **image ESP_037074_1400) and (e) Langtang crater (HiRISE image ESP_030099_1415). (f) Alcoves formed in Los crater by headward**
218 **erosion into the crater rim. Individual alcoves formed in bedrock have multiple sub-alcoves. (HiRISE image ESP_020774_1445).**

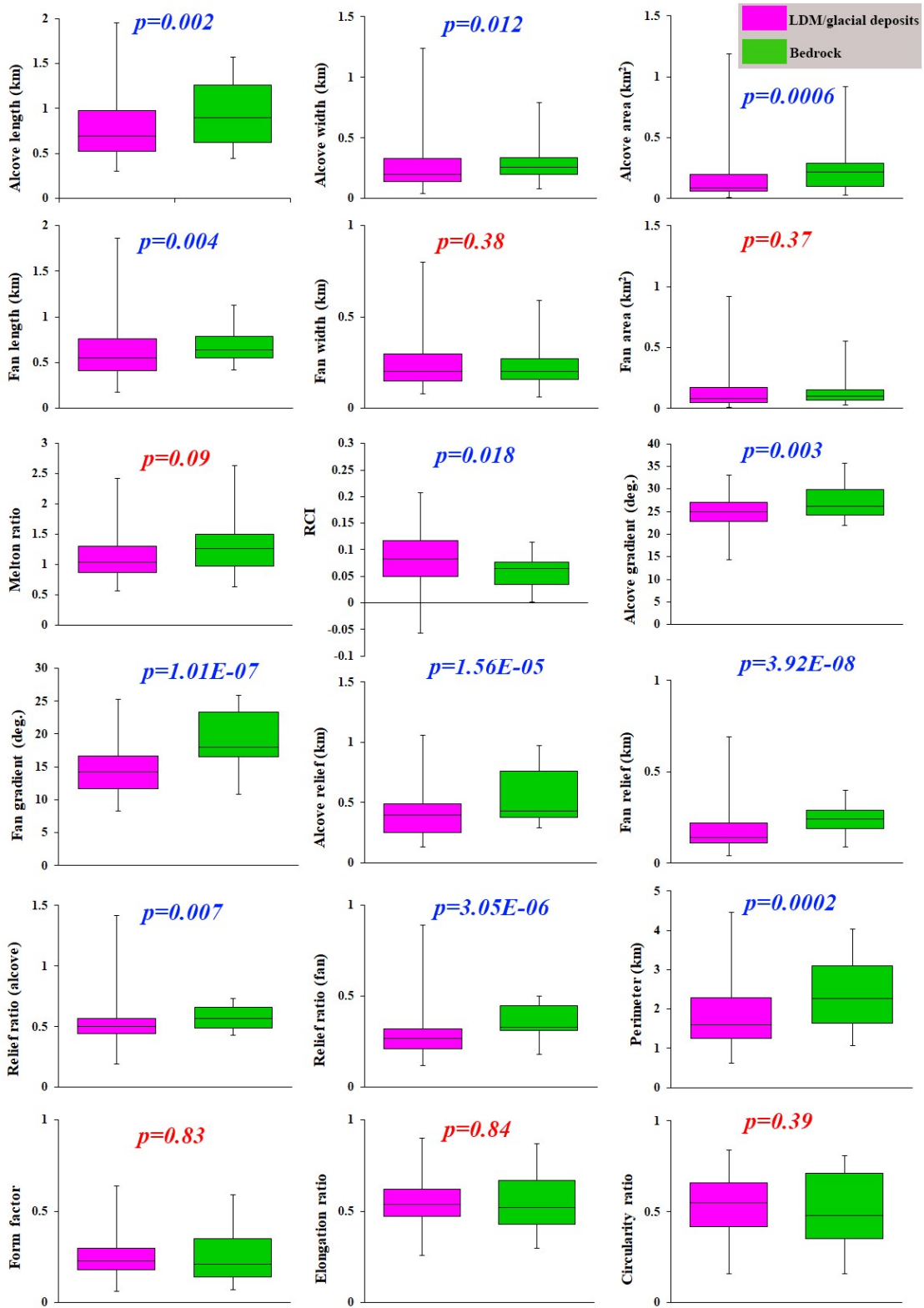
219

220 **4.2 Morphometry of gully systems**

221 Based on the criteria summarized in section 3.3, we have studied 167 gullies across 29 craters for calculation of morphometric
222 variables. 130 gullies are formed within LDM/glacial deposits, and 37 gullies are formed within the bedrock. The results of
223 morphometric calculations are summarized for visual comparison as a boxplot (Fig. 5).

224 The results of the Student’s t-test indicates that all of the morphometric variables in Table 2, except fan width, fan area, Melton
225 ratio, form factor, elongation ratio, and circularity ratio, differ significantly between LDM/glacial deposits and bedrock (Fig.
226 5). Compared to the mean gradient of gully-fans formed in LDM/glacial deposits, bedrock gully-fans are steeper and possess
227 a higher relief ratio. The interquartile range of length, relief, and perimeter of alcoves formed in bedrock are also higher than
228 the interquartile range of similar variables in LDM/glacial deposits, but the alcoves in LDM/glacial deposits possess much
229 higher values of length, relief, and perimeter (Fig. 5).

230

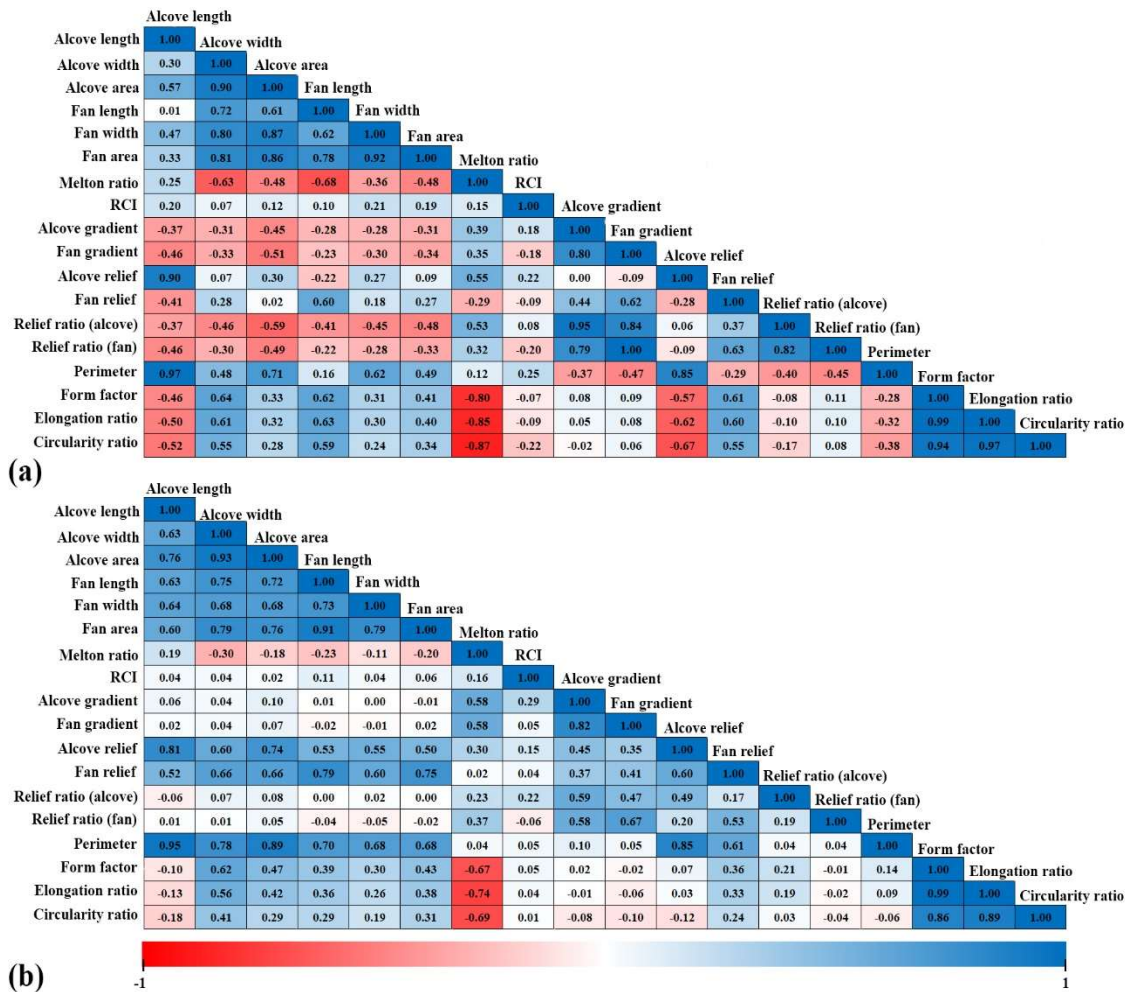


233 Figure 5: Boxplots showing the range of values of alcove/fan geometry, relief, gradient, and dimensionless variables of gullies incised
 234 into LDM/glacial deposits (pink) and bedrock (green). P-values on the plots represent the results of the student's t-tests for testing
 235 the significance of difference in means of the morphometric variables between gully systems formed on LDM/Glacial deposits and
 236 bedrock. P-values in blue correspond to significant difference (with respect to a p-value of 0.05) and those in red are non-significant.

237

238 Correlations between morphometric attributes of alcoves and fans formed in bedrock and LDM/glacial deposits are
 239 summarized in Fig. 6. For bedrock, there are strong positive correlations between 12 pairs of morphometric variables and
 240 strong negative correlations between 3 pairs of morphometric variables. For LDM/glacial deposits, there are strong positive
 241 correlations between 18 pairs of morphometric variables and strong negative correlations between 3 pairs of morphometric
 242 variables. Very strong positive correlations are found between 9 pairs of morphometric variables for bedrock and between 4
 243 pairs of morphometric variables for LDM/glacial deposits.

244



245 **Figure 6: Correlations between morphometric attributes of alcoves and fans formed in (a) bedrock and (b) LDM/glacial deposits.**
246 **Higher the value of the correlation coefficient, higher is the strength of the correlation.**

247

248 The canonical discriminant analysis reveals that the following morphometric variables best distinguish between the gully
249 systems formed in LDM/glacial deposits and bedrock, in descending order of importance: alcove perimeter, alcove relief, fan
250 gradient, fan relief, fan length, relief ratio (alcove), alcove width, relief ratio (fan), alcove gradient, alcove area, alcove length,
251 and relative concavity index (Table 3). The alcove perimeter is most important in discriminating among the gully systems
252 formed within LDM/glacial deposits and bedrock, and the next two most important variables are alcove relief and fan gradient.
253 Alcove relief and fan gradient have 4/5 and 1/3 the weight of alcove perimeter, respectively. The remaining variables such as
254 fan relief, fan length, relief ratio (alcove), alcove width, and relief ratio (fan) have nearly 1/5 the weight of alcove perimeter
255 or greater (but less than 1/3) discriminatory power in separating between the gullies formed in LDM/glacial deposits and
256 bedrock. The variables with the smallest magnitude, alcove gradient, alcove area, alcove length and relative concavity index,
257 have less than 1/10 the weight of the most important variable in separating the gully systems.

258 **Table 3.** Standardised canonical discriminant function coefficients (F1) that best separate gully systems formed on
259 LDM/Glacial deposits and bedrock.

Variable	F1
Perimeter	3.552
Alcove relief	-2.828
Fan gradient	1.278
Fan length	-1.06
Fan relief	1.06
Relief ratio (alcove)	0.971
Alcove width	-0.692
Relief ratio (fan)	-0.665
Alcove gradient	-0.331
Alcove area	-0.319
Alcove length	0.23
Relative concavity index	-0.182

260

261 **5 Discussions**

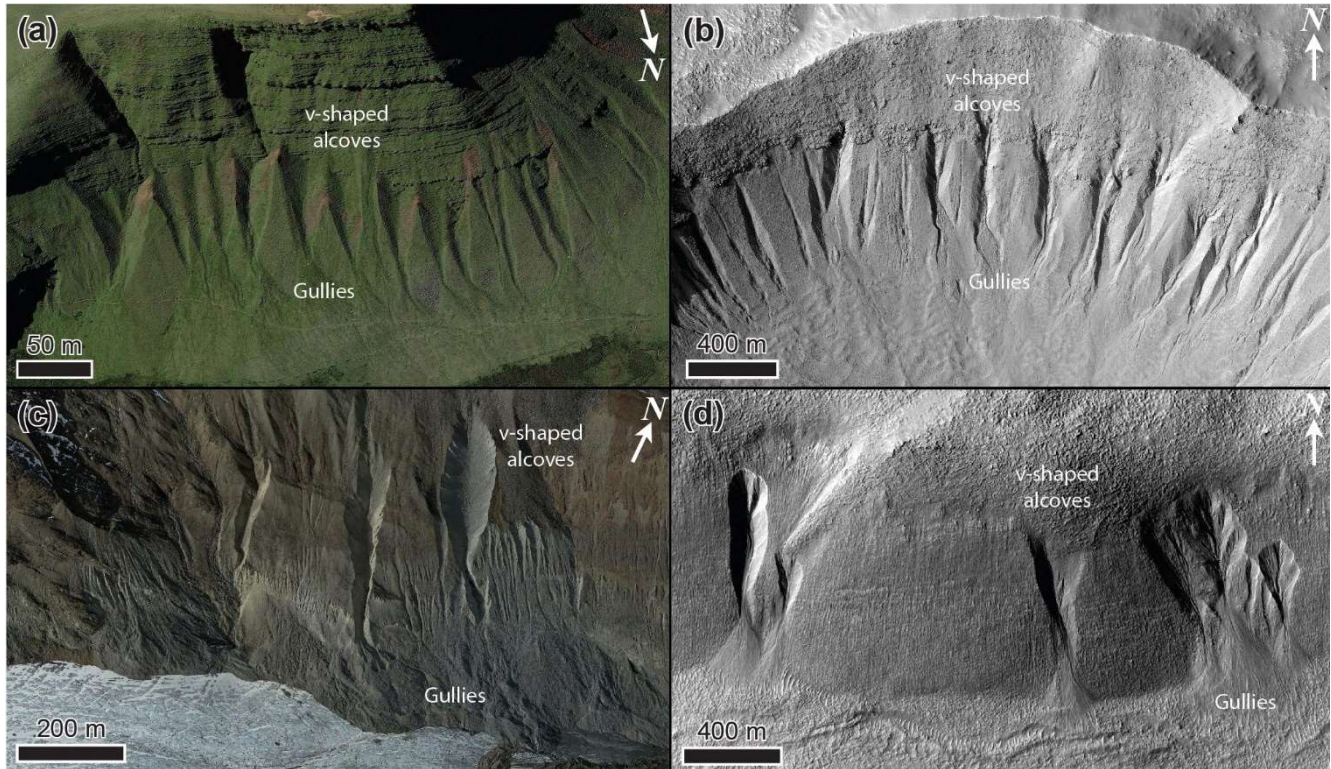
262 **5.1 Unique morphology and morphometry of gully systems in different substrates**

263 We have found that the gully systems formed in LDM/glacial deposits and bedrock can, using discriminatory analysis, be
264 distinguished from one another in terms of perimeter and relief of alcoves (Table 3). Additionally, we have found statistically
265 significant difference between the perimeter and relief of alcoves formed in LDM/glacial deposits and bedrock (Fig. 5). It is
266 likely that these differences in the perimeter and relief of alcoves formed within morphologically distinct substrates could be
267 due to the integral nature of the surface material within which the alcoves have formed. In other words, it is possible that the
268 differences in the physical properties of the sediments (namely grain size, compactness etc.) within which alcoves have formed
269 played a key role in erosion of the substrate leading to differences in their morphometric variables. Below we elaborate on the
270 uniqueness of the substrates within which alcoves have formed, and discuss further the relationships between the morphometric
271 variables of the morphologically distinct gully systems.

272 On Mars, VFFs contain high purity glacial ice with a debris cover (Sharp, 1973; Squyres, 1978, 1979; Squyres and Carr, 1986;
273 Holt et al 2008, Plaut et al 2009, Petersen et al. 2018). Their surfaces have been interpreted to be comprised of finer, reworked
274 debris derived from sublimation of the underlying ice (Mangold, 2003; Levy et al., 2009a; Morgan et al., 2009). The smooth,
275 meters thick draping unit on the walls of formerly glaciated craters has been suggested to be derived from the atmosphere as a
276 layer of dust-rich ice primarily constituting of fine-grained materials (Kreslavsky and Head, 2000; Mustard et al., 2001). The
277 fine-grained materials are loosely-packed, unconsolidated materials exhibiting low thermal inertia values (Mellon et al., 2000;
278 Putzig et al., 2005). Typically, gullies formed within this substrate display a smooth surface texture, wherein, evidence of
279 individual clasts or meter-scale boulders is not resolvable in HiRISE images, substantiating the dominant component of fine-
280 grained materials within the LDM (e.g., Levy et al., 2010; de Haas et al., 2015a). Additionally, it has been found that alcoves
281 incised into the LDM always have a distinctive V-shaped cross section in their mid-section (Figures 4d and 4e), which when
282 compared with similar-scaled systems on Earth also corresponds to the presence of loose sediments constituting the LDM
283 (Conway et al., 2018). The alcoves with V-shaped cross sections are found to be elongated, likely indicating incision within
284 ice-rich unlithified sediments (Aston et al., 2011). In the studied craters, we have found that gullies incised into LDM/glacial
285 deposits are having an elongated, V-shaped cross section in their mid-section (Fig. 4). We propose that the presence of fine-
286 grained, loosely packed, unconsolidated materials within LDM/glacial deposits has facilitated formation of elongated alcoves
287 with perimeter and relief relatively higher than that of alcoves formed in coarse-grained bedrock substrate. This is consistent
288 with the previous studies suggesting that gullies eroding into LDM/glacial deposits have elongated catchments, whereas gullies
289 eroding into the bedrock have more amphitheater-shaped catchments (Levy et al., 2009b). For this reason, the estimated length
290 of alcoves formed in LDM/glacial deposits is found to be relative higher than that of alcoves formed in bedrock (Fig. 5).
291 Furthermore, statistical analysis has revealed a significant difference between the length of alcoves formed in LDM/glacial
292 deposits and bedrock (Fig. 5). Additionally, the presence of finer-grained sediments in LDM/glacial deposits is the likely cause

293 of the V-shape of the incision of alcoves investigated in this study (Aston et al., 2011). On Earth, V-shaped incisions through
294 glacial ice-rich moraines have been observed to have occurred during the paraglacial phase of glacial retreat (Bennett et al.,
295 2000; Ewertowski and Tomczyk, 2015) (Fig. 7). The paraglacial phase refers to a terrestrial post-glacial period that represents
296 the response of changing environment to deglaciation (Bennett et al., 2000; Ewertowski and Tomczyk, 2015).

297



298

299 **Figure 7: Gullies forming in glacial sediments in deglaciated terrain in the (a) Brecon Beacons, Wales, UK on Earth (Google Earth**
300 **coordinates: 51°52'59.11"N, 3°43'33.26"W), (b) Talu crater (https://www.uahirise.org/ESP_011817_1395) on Mars, (c)**
301 **Hintereisferner, Austria (Google Earth coordinates: 46°48'54.25"N, 10°47'8.18"E), on Earth, and (d) Bunnik crater**
302 **(https://www.uahirise.org/ESP_047044_1420) on Mars. HiRISE image credit: NASA/JPL-Caltech/University of Arizona.**

303

304 The next most important difference between these two types of gullies is the mean gradient of gully fans. At the foot of the
305 fans, mean gradient of the fans influenced by LDM/glacial deposits is $<15^\circ$ for 61% of the studied fans. For bedrock, 84% of
306 the studied fans have a mean gradient $>15^\circ$ at the foot of the fans. Hence, gully-fans formed in bedrock are emplaced at a
307 relatively steeper gradient than the fans formed from gullies in LDM/glacial deposits. We propose that the nature of the material

308 mobilized can explain this difference, with the finer-grained sediments characteristic of the LDM/glacial type gullies being
309 easier to mobilise and being entrained to lower slope angles, than the coarser sediments found within the bedrock type gullies.

310 **5.2 Evaluation of the gully formation process**

311 On Earth, alcove-fan systems can roughly be subdivided in flood-dominated, debris-flow dominated, and colluvial systems.

312 Following the terminology of De Haas et al., (2015b) and Tomczyk (2021), we define these systems as follows:

313 1) Flood-dominated systems: These are systems dominated by fluid-gravity flows, i.e., water floods, hyperconcentrated floods,
314 and debris floods. The fans of such systems are commonly referred to as fluvial or alluvial fans (e.g., Ryder, 1971; Blair and
315 McPherson, 1994; Hartley et al., 2005).

316 2) Debris-flow dominated systems: These are systems dominated by sediment-gravity flows, i.e., debris flows, mud flows.
317 Irrespective of their radial extent and depositional gradients, the fans aggraded by these systems can be commonly called
318 debris-flow fans or debris fans (Blikra and Nemeč, 1998; de Scally et al., 2010).

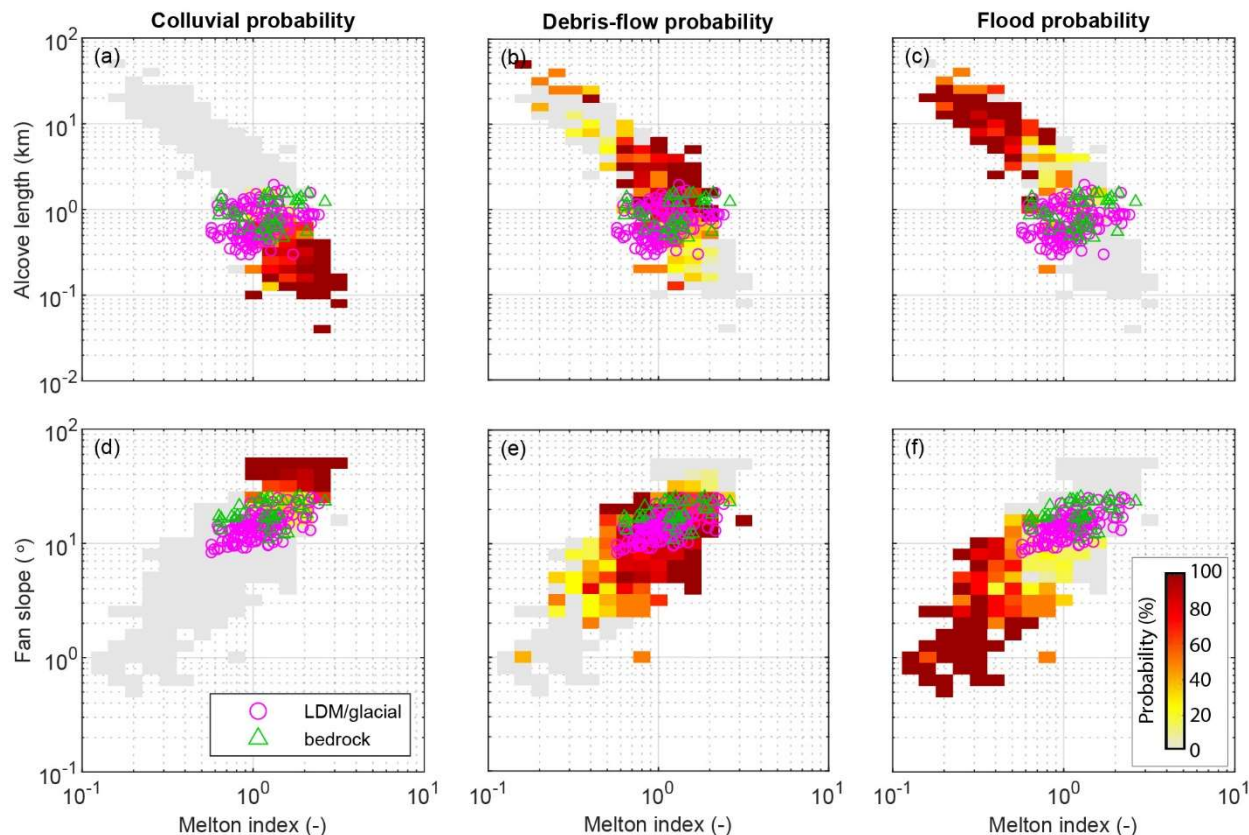
319 3) Colluvial systems: These are systems dominated by rock-gravity and sediment-gravity flows, with their dominant activity
320 relating to rockfalls, grain flows, and snow avalanches (in periglacial and alpine settings). Debris flows typically constitute
321 only a relatively minor component of geomorphic processes in such systems. The fans of these systems are also commonly
322 known as colluvial cones or talus cones (Siewert et al., 2012; De Haas et al., 2015b).

323 Although these systems may be dominated by one type of geomorphic process, it is important to stress that other processes
324 may also occur. For example, on Earth water floods are not uncommon on many debris-flow dominated systems, while debris-
325 flow deposits are commonly recognized on colluvial cones.

326

327

328



330

331 **Figure 8: Comparison of combinations of Melton ratio with Alcove length and Fan gradient. The probability heat maps**
 332 **are based on previously published data – see text for references. The Martian gully systems formed in LDM/glacial**
 333 **deposits and bedrock are found to be in the debris-flow regime on Earth. The gray area shows the realm of the colluvial,**
 334 **debris-flow, and fluvial fans together.**

335

336 To compare the morphometric characteristics of the Martian gully systems to terrestrial systems, we have compiled
 337 morphometric data of alcoves and fans across several continents, mountain ranges, climate zones, and process types on Earth.
 338 This dataset includes published data from the Himalayas, Ladakh, India (Stolle et al., 2013), the tropical Andes, Columbia
 339 (Arango et al., 2021), Spitsbergen, Svalbard (Tomczyk, 2021), British Columbia, Canada (Kostaschuk, 1986; Jackson et al.,
 340 1987; and newly presented data), the southern Carpathians, Romania (Ilinca et al., 2021), the Southern Alps, New Zealand (De
 341 Scally and Owens, 2004; De Scally et al., 2010), the North Cascade Foothills, USA, the European Alps (including Switzerland,
 342 Italy, France, and Austria), and the Pyrenees (from multiple authors compiled by Bertrand et al., 2013). The dataset comprises
 343 information from colluvial, debris-flow, and flood (also including debris flood) dominated systems. In total, it contains 231

344 colluvial systems, 749 debris-flow dominated systems, and 369 flood-dominated systems. In total, data were compiled for
345 1349 systems, although not all information was available for all systems, with data availability ranging from 729 sites for
346 alcove length to all 1349 systems for Melton index and process type. Based on this data we have made a heatmap of the
347 probability of flood, debris-flow, or colluvially-dominated conditions for combinations of Melton ratio with alcove length and
348 fan gradient, to which we compare the Martian gullies (Fig. 8). We have specifically chosen the combinations of Melton ratio
349 with alcove length and fan gradient to infer the Martian gully formative mechanism because they have been widely used in
350 discriminating terrestrial drainage basins and fans prone to flooding from those subject to debris flows, debris floods and floods
351 (e.g. De Scally and Owens, 2004; Wilford et al., 2004). We have found that the Martian gullies are indeed in the debris-flow
352 regime on Earth. Moreover, they are closer to the transition to the smaller and steeper colluvial cones than to transition to
353 flood-dominated fans. As expected, bedrock systems in Fig. 8d-e are closer to the colluvial systems than the LDM systems.

354

355 According to the previous reports of debris-flow like deposits found in Martian gullies (e.g. Johnsson et al., 2014; Sinha et al.,
356 2019, 2020), the morphological attributes of debris-flow like deposits typically include overlapping tongue-shaped lobes with
357 embedded clasts, channels with medial deposits, and channels with clearly defined lateral levees. Although it is still not clear
358 whether the formation of these deposits in gullies are from sublimation of CO₂ ice or due to meltwater generation. De Haas et
359 al., (2019b) showed that CO₂ sublimation may lead to flow fluidization on Mars in a manner similar to fluidization by water
360 in terrestrial debris flows; a concept supported by the recent finding of lobate deposits and boulder-rich levee formation during
361 the present-day in Istok crater (Table 1) (Dundas et al., 2019). The formation of these morphologically similar deposits during
362 the present-day is attributed to sublimating CO₂ frost, which likely produces the necessary fluidization likely by gas generated
363 from entrained CO₂ frost (Dundas et al., 2019). On the basis of these recent reports (De Haas et al., 2019b; Dundas et al., 2019)
364 and based on our own findings in this study, we argue that a debris-flow like process similar to those operated in the terrestrial
365 gully systems has likely dominated the flow types that lead to gully formation on Mars. It is likely that the present-day
366 sublimation of CO₂ ice on Mars provided the necessary flow fluidization for the emplacement of deposits similar to terrestrial
367 debris-flow like deposits (De Haas et al., 2019b).

368 **6 Conclusions**

369 This paper compares morphological and morphometric characteristics of gully alcoves and associated fans formed in
370 LDM/glacial deposits and bedrock over walls of 29 craters between 30° S and 75° S latitudes. 5 craters out of 29 have alcoves-
371 fans formed within the bedrock and remaining 24 craters have alcoves-fans formed within LDM/glacial deposits. From our
372 analysis of 167 gullies, we posit that gully systems formed in LDM/glacial deposits and bedrock differ from one another using
373 the following lines of evidence:

374 • Alcoves formed in LDM/glacial deposits are more elongated than the alcoves formed in bedrock, and possess a distinctive
375 V-shaped cross section.

376 • The mean gradient of gully-fans formed in bedrock is steeper than the mean gradient of fans formed from gullies in
377 LDM/glacial deposits.

378 The morphological distinction reported between gullies formed in the bedrock and LDM/glacial deposits signifies that Martian
379 gullies may have multiple formative mechanisms. We infer that the presence of mantling material could be one of the key
380 factors in constraining the mechanisms forming Martian gully systems and that presence of LDM would promote formation
381 of elongated alcoves with perimeter and relief relatively higher than that of alcoves formed in coarse-grained bedrock substrate.

382 Based on the combinations of Melton ratio with alcove length and fan gradient, we suggest that the gully systems studied in
383 this work were likely dominated by terrestrial debris-flow like processes during their formation. This is consistent with the
384 findings reported in previous studies that showed evidence of formation of deposits morphologically similar to terrestrial
385 debris-flow like deposits, both in the past and during the present-day (e.g., Johnsson et al., 2014; Dundas et al., 2019). The
386 present-day sublimation of CO₂ ice on Mars is envisaged to provide the necessary flow fluidization for the emplacement of
387 deposits similar to debris-flow like deposits on Earth (De Haas et al., 2019b).

388 **7 Author contribution**

389 RKS, TDH and SJC conceptualized this work. The methodology was developed by RKS, TDH and SJC. Data curation and
390 formal analyses were performed by RKS. TDH and AN also contributed in collection of datasets used in this work. RKS, DR,
391 TDH and SJC contributed to the interpretation of the data and results. RKS wrote the original draft of this paper, which was
392 reviewed and edited by all authors.

393 **8 Conflict of interest**

394 SJC is a Guest Editor of this special issue (Planetary landscapes, landforms, and their analogues) of ESurfD and on the editorial
395 board for ESurf. The peer-review process was guided by an independent editor, and the authors have also no other competing
396 interests to declare.

397 **9 Acknowledgements**

398 We are grateful and thank both the anonymous reviewers for thorough assessment of our manuscript and for providing us
399 constructive comments and suggestions. Thanks to the Editor (Heather Viles) and Associate Editor (Frances E. G. Butcher) at
400 Earth Surface Dynamics for the editorial handling of the manuscript. We would like to thank the HiRISE team for their work
401 to produce the images and digital elevation models used in this study, it would have been impossible without them. RKS and
402 DR acknowledge the financial support by the Indian Space Research Organisation, Department of Space, Government of India.

403 SJC and AN are grateful for the financial support from Région Pays de la Loire, project étoiles montantes METAFLOWS
404 (convention N° 2019-14294) and also the financial support of CNES in support of their HiRISE work. TdH was supported by
405 the Netherlands Organisation for Scientific Research (NWO) (grant 016.Veni.192.001). We acknowledge the efforts of team
406 MUTED to develop an online tool (<http://muted.wvu.de/>) for quick identification of the spatial and multi-temporal coverage
407 of planetary image data from Mars. All the planetary datasets used in this work are available for free download at the PDS
408 Geosciences Node Mars Orbital Data Explorer (ODE) (<https://ode.rsl.wustl.edu/mars/>) and <https://www.uahirise.org/>. The
409 newly-generated DTMs can be downloaded from https://figshare.com/articles/dataset/Self_generated_DEMs/21717164.
410 The measurement datasets can be downloaded from
411 [https://figshare.com/articles/dataset/Measurement_data_of_gully_systems_in_the_southern_mid_latitudes_of_Mars/](https://figshare.com/articles/dataset/Measurement_data_of_gully_systems_in_the_southern_mid_latitudes_of_Mars/21717182)
412 **21717182**. This work is a part of the PhD work of Rishitosh K. Sinha. Director PRL, Head of Planetary Science Division,
413 PRL, Head of Planetary Remote Sensing Section, PRL, and Director IIT Gandhinagar are gratefully acknowledged for constant
414 encouragement during the work.

415 **References**

- 416 Arango, M. I., Aristizábal, E., & Gómez, F.: Morphometrical analysis of torrential flows-prone catchments in tropical and
417 mountainous terrain of the Colombian Andes by machine learning techniques, *Natural Hazards*, 105(1), 983-1012, doi:
418 <https://doi.org/10.1007/s11069-020-04346-5>, 2021.
- 419 Arfstrom, J. & Hartmann, W.K.: Martian flow features, moraine-like ridges, and gullies: terrestrial analogs and
420 interrelationships, *Icarus*, 174, 321–335, doi: <https://doi.org/10.1016/j.icarus.2004.05.026>, 2005.
- 421 Aston, A., Conway, S. & Balme, M.: Identifying Martian Gully Evolution. In: Balme, M.R., Bargery, A.S., Gallagher, C.J. &
422 Gupta, S. (eds) *Martian Geomorphology*, Geological Society, London, Special Publications, 356, 151–169, doi:
423 <https://doi.org/10.1144/SP356.9>, 2011.
- 424 Balme, M., Mangold, N. Et Al.: Orientation and distribution of recent gullies in the southern hemisphere of Mars: observations
425 from High Resolution Stereo Camera/Mars Express (HRSC/MEX) and Mars Orbiter Camera/Mars Global Surveyor
426 (MOC/MGS) data, *J. Geophys. Res.: Planets*, 111, E05001, doi: <https://doi.org/10.1029/2005JE002607>, 2006.
- 427 Bertrand, M., Liébault, F., & Piégay, H.: Debris-flow susceptibility of upland catchments, *Natural Hazards*, 67(2), 497-511,
428 doi: <https://doi.org/10.1007/s11069-013-0575-4>, 2013.
- 429 Blair, T.C. & Mcpherson, J.G.: Processes and forms of alluvial fans. In: PARSONS, A. & ABRAHAMMS, A. (eds)
430 *Geomorphology of Desert Environments*, Springer, Dordrecht, The Netherlands, 413–467, doi: [https://doi.org/10.1007/978-1-](https://doi.org/10.1007/978-1-4314020-5719-9_14)
431 [4020-5719-9_14](https://doi.org/10.1007/978-1-4314020-5719-9_14), 2009.

432 Blair, T.C.: Sedimentology of the debris-flow-dominated Warm Spring Canyon alluvial fan, Death Valley, California,
433 Sedimentology 46 (5), 941–965, doi: <https://doi.org/10.1046/j.1365-3091.1999.00260.x>, 1999.

434 Blikra, L.H., Nemeč, W.: Postglacial colluvium in western Norway: depositional processes, facies and palaeoclimatic record.
435 Sedimentology 45 (5), 909–960, doi: <https://doi.org/10.1046/j.1365-3091.1998.00200.x>, 1998.

436 Cedillo-Flores, Y., Treiman, A.H., Lasue, J. & Clifford, S.M.: CO₂ gas fluidization in the initiation and formation of Martian
437 polar gullies, Geophys. Res. Letters, 38, L21202 doi: <https://doi.org/10.1029/2011GL049403>, 2011.

438 Christensen, P.R.: Formation of recent Martian gullies through melting of extensive water-rich snow deposits, Nature, 422,
439 45–48, doi: <https://doi.org/10.1038/nature01436>, 2003.

440 Conway, S. J., Butcher, F. E., de Haas, T., Deijns, A. A., Grindrod, P. M., & Davis, J. M.: Glacial and gully erosion on Mars:
441 A terrestrial perspective, Geomorphology, 318, 26–57, doi: <https://doi.org/10.1016/j.geomorph.2018.05.019>, 2018.

442 Conway, S.J. & Balme, M.R.: Decameter thick remnant glacial ice deposits on Mars, Geophys. Res. Letters, 41, 5402–5409,
443 doi: <https://doi.org/10.1002/2014GL060314>, 2014.

444 Conway, S.J., Balme, M.R., Kreslavsky, M.A., Murray, J.B. & Towner, M.C.: The comparison of topographic long profiles
445 of gullies on Earth to gullies on Mars: a signal of water on Mars. Icarus, 253, 189–204, doi:
446 <https://doi.org/10.1016/j.icarus.2015.03.009>, 2015.

447 Conway, S.J., Balme, M.R., Murray, J.B., Towner, M.C., Okubo, C.H. & Grindrod, P.M.: The indication of Martian gully
448 formation processes by slope–area analysis, In: Balme, M.R., Bargery, A.S., Gallagher, C.J. & Gupta, S. (eds) Martian
449 Geomorphology, Geological Society, London, Special Publications, 356, 171–201, doi: <https://doi.org/10.1144/SP356.10>,
450 2011.

451 Conway, S.J., Harrison, T.N., Soare, R.J., Britton, A.W. & Steele, L.J.: New slope-normalized global gully density and
452 orientation maps for Mars, In: Conway, S.J., Carrivick, J.L., Carling, P.A., De Haas, T. & Harrison, T.N. (eds) Martian Gullies
453 and their Earth Analogues, Geol. Soc. Lond. Spec. Publ. 467. First published online November 27, 2017, doi:
454 <https://doi.org/10.1144/SP467.3>, 2017.

455 Costard, F., Forget, F., Mangold, N. & Peulvast, J.P.: Formation of recent Martian debris flows by melting of near-surface
456 ground ice at high obliquity, Science, 295, 110–113, doi: [10.1126/science.1066](https://doi.org/10.1126/science.1066), 2002.

457 Crosta, G.B., Frattini, P.: Controls on modern alluvial fan processes in the central Alps, northern Italy, Earth Surf. Proc. Land.
458 29 (3), 267–293, doi: <https://doi.org/10.1002/esp.1009>, 2004.

459 de Haas, T., Conway, S.J., Butcher, F.E.G., Levy, J.S., Grindrod, P.M., Balme, M.R., Goudge, T.A.: Time will tell: temporal
460 evolution of Martian gullies and paleoclimatic implications, *Geol. Soc. Lond. Spec. Publ.* 467, doi:
461 <https://doi.org/10.1144/SP467.1>, 2019a.

462 de Haas, T., McArdell, B. W., Conway, S. J., McElwaine, J. N., Kleinhans, M. G., Salese, F., & Grindrod, P. M.: Initiation
463 and flow conditions of contemporary flows in Martian gullies, *J. Geophys. Res.: Planets*, 124(8), 2246-2271, doi:
464 <https://doi.org/10.1029/2018JE005899>, 2019b.

465 de Haas, T., Hauber, E. & Kleinhans, M.G. 2013. Local late Amazonian boulder breakdown and denudation rate on Mars,
466 *Geophys. Res. Letters*, 40, 3527–3531, doi: <https://doi.org/10.1002/grl.50726>, 2013.

467 de Haas, T., Ventra, D., Hauber, E., Conway, S.J. & Kleinhans, M.G.: Sedimentological analyses of Martian gullies: the
468 subsurface as the key to the surface, *Icarus*, 258, 92–108, doi: <https://doi.org/10.1016/j.icarus.2015.06.017>, 2015a.

469 de Haas, T., Kleinhans, M. G., Carbonneau, P. E., Rubensdotter, L., & Hauber, E.: Surface morphology of fans in the high-
470 Arctic periglacial environment of Svalbard: Controls and processes, *Earth-Science Reviews*, 146, 163-182, doi:
471 <https://doi.org/10.1016/j.earscirev.2015.04.004>, 2015b.

472 de Scally, F. A., & Owens, I. F.: Morphometric controls and geomorphic responses on fans in the Southern Alps, New Zealand,
473 *Earth Surface Processes and Landforms: The Journal of the British Geomorphological Research Group*, 29(3), 311-322, doi:
474 <https://doi.org/10.1002/esp.1022>, 2004.

475 De Scally, F.A., Owens, I.F., Louis, J.: Controls on fan depositional processes in the schist ranges of the Southern Alps, New
476 Zealand, and implications for debris-flow hazard assessment, *Geomorphology* 122 (1–2), 99–116, doi:
477 <https://doi.org/10.1016/j.geomorph.2010.06.002>, 2010.

478 Dickson, J.L. & Head, J.W.: The formation and evolution of youthful gullies on Mars: gullies as the latestage phase of Mars
479 most recent ice age, *Icarus*, 204, 63–86, doi: <https://doi.org/10.1016/j.icarus.2009.06.018>, 2009.

480 Dickson, J.L. et al.: Recent climate cycles on Mars: Stratigraphic relationships between multiple generations of gullies and the
481 latitude dependent mantle, *Icarus* 252, 83–94, doi: <http://dx.doi.org/10.1016/j.icarus.2014.12.035>, 2015.

482 Dickson, J.L., Head, J.W., Fassett, C.I.: Patterns of accumulation and flow of ice in the mid-latitudes of Mars during the
483 Amazonian, *Icarus* 219, 723–732, doi: <http://dx.doi.org/10.1016/j.icarus.2012.03.010>, 2012.

484 Dickson, J.L., Head, J.W., Kreslavsky, M.: Martian gullies in the southern midlatitudes of Mars: Evidence for climate-
485 controlled formation of young fluvial features based upon local and global topography, *Icarus* 188, 315–323, doi:
486 <https://doi.org/10.1016/j.icarus.2006.11.020>, 2007.

487 Dundas, C. M., McEwen, A. S., Diniega, S., Hansen, C. J., Byrne, S., & McElwaine, J. N.: The formation of gullies on Mars
488 today, *Geol. Soc. Lond. Spec. Publ.* 467, 67-94, doi: <https://doi.org/10.1144/SP46>, 2019.

489 Dundas, C.M., Diniega, S., Hansen, C.J., Byrne, S., McEwen, A.S.: Seasonal activity and morphological changes in martian
490 gullies, *Icarus* 220:124–143, doi: <https://doi.org/10.1016/j.icarus.2012.04.005>, 2012.

491 Dundas, C.M., Diniega, S., McEwen, A.S.: Long-term monitoring of Martian gully formation and evolution with
492 MRO/HiRISE, *Icarus* 251:244–263, doi: <https://doi.org/10.1016/j.icarus.2014.05.013>, 2015.

493 Hargitai, H. (2014). Viscous Flow Features (Mars). In: *Encyclopedia of Planetary Landforms*. Springer, New York, NY.
494 https://doi.org/10.1007/978-1-4614-9213-9_596-1

495 Harrison, T.N., Osinski, G.R., Tornabene, L.L., Jones, E.: Global documentation of gullies with the Mars reconnaissance
496 orbiter context camera and implications for their formation, *Icarus* 252:236–254, doi:
497 <https://doi.org/10.1016/j.icarus.2015.01.022>, 2015.

498 Hartley, A.J., Mather, A.E., Jolley, E., Turner, P.: Climatic controls on alluvial-fan activity, Coastal Cordillera, northern Chile.
499 In: Harvey, A.M., Mather, A.E., Stokes, M. (Eds.), *Alluvial Fans: Geomorphology, Sedimentology, Dynamics*. *Geol. Soc.*
500 *Lond. Spec. Publ.* 251, 95-115, doi: <https://doi.org/10.1144/GSL.SP.2005.251.01>, 2005.

501 Head, J.W., Marchant, D.R., Dickson, J.L., Kress, A.M., Baker, D.M.: Northern midlatitude glaciation in the Late Amazonian
502 period of Mars: criteria for the recognition of debris-covered glacier and valley glacier landsystem deposits, *Earth Planet. Sci.*
503 *Lett.* 294:306–320, doi: <https://doi.org/10.1016/j.epsl.2009.06.041>, 2010.

504 HELDMANN, J.L. & MELLON, M.T.: Observations of Martian gullies and constraints on potential formation mechanisms,
505 *Icarus*, 168, 285–304, doi: <https://doi.org/10.1016/j.icarus.2003.11.024>, 2004.

506 Heldmann, J.L. et al.: Formation of martian gullies by the action of liquid water flowing under current martian environmental
507 conditions, *J. Geophys. Res. Planets* 110, doi: <http://dx.doi.org/10.1029/2004JE002261>, 2005.

508 Hobbs, S.W., Paull, D.J., Clark, J.D.A.: A comparison of semiarid and subhumid terrestrial gullies with gullies on Mars:
509 Implications for martian gully erosion, *Geomorphology* 204, 344–365, doi: <http://dx.doi.org/10.1016/j.geomorph.2013.08.018>,
510 2014.

511 Hobbs, S.W., Paull, D.J. and Clarke, J.D.A.: Analysis of regional gullies within Noachis Terra, Mars: A complex relationship
512 between slope, surface material and aspect, *Icarus*, 250, 308-331, doi: <https://doi.org/10.1016/j.icarus.2014.12.011>, 2015.

513 Hubbard, B., Milliken, R.E., Kargel, J.S., Limaye, A. & Souness, C.: Geomorphological characterisation and interpretation of
514 a mid-latitude glacier-like form: Hellas Planitia, Mars, *Icarus*, 211, 330–346, doi: <https://doi.org/10.1016/j.icarus.2010.10.021>,
515 2011.

516 Ilinca, V.: Using morphometrics to distinguish between debris flow, debris flood and flood (Southern Carpathians, Romania),
517 *Catena*, 197, 104982, doi: <https://doi.org/10.1016/j.catena.2020.104982>, 2021.

518 Jackson LE, Kostaschuk RA, MacDonald GM: Identification of debris flow hazard on alluvial fans in the Canadian Rocky
519 Mountains, In: Costa JE, Wieczorek GF (eds) *Debris flows/avalanches: process, recognition, and mitigation*. *Rev Eng Geol*
520 vol. VII. *Geol. Soc. Am*, doi: <https://doi.org/10.1130/REG7-p115>, 1987.

521 Johnsson, A. et al.: Evidence for very recent melt-water and debris flow activity in gullies in a young mid-latitude crater on
522 Mars, *Icarus* 235, 37–54, doi: <http://dx.doi.org/10.1016/j.icarus.2014.03.005>, 2014.

523 Kirk, R.L., Howington-Kraus, E., Rosiek, M.R., Anderson, J.A., Archinal, B.A., Becker, K.J., Cook, D.A., Galuszka, D.M.,
524 Geissler, P.E., Hare, T.M., Holmberg, I.M., Keszthelyi, L.P., Redding, B.L., Delamere, W.A., Gallagher, D., Chapel, J.D.,
525 Eliason, E.M., King, R., McEwen, A.S.: Ultrahigh resolution topographic mapping of Mars with MRO HiRISE stereo images:
526 meter-scale slopes of candidate Phoenix landing sites, *J. Geophys. Res. Planets* 113, doi:
527 <https://doi.org/10.1029/2007JE003000>, 2008.

528 Kostaschuk, R.A., Macdonald, G.M., Putnam, P.E.: Depositional process and alluvial fan-drainage basin morphometric
529 relationships near Banff, Alberta, Canada, *Earth Surf. Proc. Land.* 11 (5), 471–484, doi:
530 <https://doi.org/10.1002/esp.3290110502>, 1986.

531 Kreslavsky, M.A.: Slope steepness of channels and aprons: Implications for origin of martian gullies. *Workshop Martian*
532 *Gullies, Workshop on Martian Gullies 2008*. Abs.#1301, 2008.

533 Kreslavsky, M.A., Head, J.W.: Mars: nature and evolution of young latitudedependent water-ice-rich mantle, *Geophys. Res.*
534 *Lett.* 29, doi: <https://doi.org/10.1029/2002GL015392>, 2002.

535 Langbein, W. B.: Profiles of rivers of uniform discharge, *U.S. Geol. Surv. Prof. Pap.*, 501-B, 119– 122, doi:
536 <https://doi.org/10.1086/627653>, 1964.

537 Lanza, N. L., Meyer, G. A., Okubo, C. H., Newsom, H. E., & Wiens, R. C.: Evidence for debris flow gully formation initiated
538 by shallow subsurface water on Mars, *Icarus*, 205(1), 103-112, doi: <https://doi.org/10.1016/j.icarus.2009.04.014>, 2010.

539 Levy, J.S. et al.: Identification of gully debris flow deposits in Protonilus Mensae, Mars: Characterization of a water-bearing,
540 energetic gully-forming process, *Earth Planet. Sci. Lett. Mars Express after 6 Years in Orbit: Mars Geology from Three-*
541 *Dimensional Mapping by the High Resolution Stereo Camera (HRSC) Experiment 294*, 368–377, doi:
542 <https://doi.org/10.1016/j.epsl.2009.08.002>, 2010b.

543 Levy, J.S., Head, J., Marchant, D.: Thermal contraction crack polygons on Mars: classification, distribution, and climate
544 implications from HiRISE observations, *J. Geophys. Res. Planets* 114, 01007, doi: <https://doi.org/10.1029/2008JE003273>,
545 2009a.

546 Levy, J. S., Head, J. W., Marchant, D. R., Dickson, J. L., & Morgan, G. A.: Geologically recent gully–polygon relationships
547 on Mars: Insights from the Antarctic Dry Valleys on the roles of permafrost, microclimates, and water sources for surface
548 flow, *Icarus*, 201(1), 113–126, doi: <https://doi.org/10.1016/j.icarus.2008.12.043>, 2009b.

549 Levy, J.S., Head, J.W., Marchant, D.R.: Gullies, polygons and mantles in Martian permafrost environments: cold desert
550 landforms and sedimentary processes during recent Martian geological history, *Geol. Soc. Lond. Spec. Publ.* 354, 167–182,
551 doi: <https://doi.org/10.1144/SP354.10>, 2011.

552 Malin, M.C., Edgett, K.S.: Evidence for recent groundwater seepage and surface runoff on Mars. *Science* 288:2330–2335, doi:
553 <https://doi.org/10.1126/science.288.5475.2330>, 2000.

554 McEwen, A.S., Eliason, E.M. et al.: Mars reconnaissance orbiter’s High Resolution Imaging Science Experiment (HiRISE), *J.*
555 *Geophys. Res.: Planets*, 112, E05S02, doi: <https://doi.org/10.1029/2005JE002605>, 2007.

556 Melton, M.A.: An analysis of the relation among elements of climate, surface properties and geomorphology, Office of Nav.
557 Res. Dept. Geol. Columbia Univ, NY. Tech. Rep. 11, 1975.

558 Milliken, R.E., Mustard, J.F., Goldsby, D.L.: Viscous flow features on the surface of Mars: observations from high-resolution
559 Mars Orbiter Camera (MOC) images, *J. Geophys. Res.* 108, doi: <https://doi.org/10.1029/2002JE002005>, 2003.

560 Mustard, J.F., Cooper, C.D., Rifkin, M.K.: Evidence for recent climate change on Mars from the identification of youthful
561 near-surface ground ice, *Nature* 412:411–414, doi: <https://doi.org/10.1038/35086515>, 2001.

562 Phillips, J.D., Lutz, J.D.: Profile convexities in bedrock and alluvial streams, *Geomorphology* 102, 554–566, doi:
563 <https://doi.org/10.1016/j.geomorph.2008.05.042>, 2008.

564 Pilonget, C. & Forget: Formation of gullies on mars by debris flows triggered by CO2 sublimation, *Nature Geoscience*, 9, 65–
565 69, doi: <https://doi.org/10.1038/ngeo2619>, 2016.

566 Reiss, D. et al.: Absolute dune ages and implications for the time of formation of gullies in Nirgal Vallis, Mars. *J. Geophys.*
567 *Res.-Planets* 109, doi: <http://dx.doi.org/10.1029/2004JE002251>, 2004.

568 Reiss, D., Hauber, E. et al.: Terrestrial gullies and debris-flow tracks on Svalbard as planetary analogs for Mars, In: Garry,
569 W.B. & Bleacher, J.E. (eds) *Analogues for Planetary Exploration*, *Geol. Soc. Am. Spec. Papers* 483, 165–175, doi:
570 [https://doi.org/10.1130/2011.2483\(11\)](https://doi.org/10.1130/2011.2483(11)), 2011.

571 Rodine, J.D., Johnson, A.M.: The ability of debris, heavily freighted with coarse clastic materials, to flow on gentle slopes,
572 *Sedimentology* 23, 213–234, doi: <https://doi.org/10.1111/j.1365-3091.1976.tb00047.x>, 1976.

573 Ryder, J.: Some aspects of the morphometry of paraglacial alluvial fans in South-central British Columbia, *Canadian Journal*
574 *of Earth Sciences* 8: 1252–1264, doi: <https://doi.org/10.1139/e71-11>, 1971.

575 Schon, S.C., Head, J.W., Fassett, C.I.: Unique chronostratigraphic marker in depositional fan stratigraphy on Mars: Evidence
576 for ca. 1.25 Ma gully activity and surficial meltwater origin, *Geology* 37, 207–210, doi: <http://dx.doi.org/10.1130/g25398a.1>,
577 2009.

578 Siewert, M. B., Krautblatter, M., Christiansen, H. H., & Eckerstorfer, M.: Arctic rockwall retreat rates estimated using
579 laboratory-calibrated ERT measurements of talus cones in Longyeardalen, Svalbard, *Earth Surface Processes and Landforms*,
580 37(14), 1542-1555, doi: <https://doi.org/10.1002/esp.3297>, 2012.

581 Sinha, R. K., Ray, D., De Haas, T., & Conway, S. J.: Global documentation of overlapping lobate deposits in Martian gullies.
582 *Icarus*, 352, 113979, doi: <https://doi.org/10.1016/j.icarus.2020.113979>, 2020.

583 Sinha, R. K., Vijayan, S., Shukla, A. D., Das, P., & Bhattacharya, F.: Gullies and debris-flows in Ladakh Himalaya, India: a
584 potential Martian analogue, *Geol. Soc. Lond. Spec. Publ.* 467, 315-342, doi: <https://doi.org/10.1144/SP46>, 2019.

585 Sinha, R.K., Vijayan, S.: Geomorphic investigation of craters in Alba Mons, Mars: implications for Late Amazonian glacial
586 activity in the region, *Planet. Space Sci.* 144:32–48, doi: <https://doi.org/10.1016/j.pss.2017.05.014>, 2017.

587 Souness, C., & Hubbard, B.: Mid-latitude glaciation on Mars, *Progress in Physical Geography*, 36(2), 238-261, doi:
588 <https://doi.org/10.1177/030913331243>, 2012.

589 Souness, C., Hubbard, B., Milliken, R. E., & Quincey, D.: An inventory and population-scale analysis of martian glacier-like
590 forms, *Icarus*, 217(1), 243-255, doi: <https://doi.org/10.1016/j.icarus.2011.10.020>, 2012.

591 Stock, J.D., Dietrich, W.E.: Erosion of steepland valleys by debris flow, *Geol. Soc. Am. Bull.* 118 (9/10), 1125–1148.
592 doi:10.1130/B25902.1, 2006.

593 Stolle, A., Langer, M., Blöthe, J. H., & Korup, O.: On predicting debris flows in arid mountain belts, *Global and Planetary*
594 *Change*, 126, 1-13, doi: <https://doi.org/10.1016/j.gloplacha.2014.12.005>, 2015.

595 Welsh, A., Davies, T.: Identification of alluvial fans susceptible to debris-flow hazards. *Landslides* 8 (2), 183–194, doi:
596 <https://doi.org/10.1007/s10346-010-0238-4>, 2011.

597 Wilford, D. J., Sakals, M. E., Innes, J. L., Sidle, R. C., & Bergerud, W. A.: Recognition of debris flow, debris flood and flood
598 hazard through watershed morphometrics, *Landslides*, 1(1), 61-66, doi: <https://doi.org/10.1007/s10346-003-0002-0>, 2004.

599 Yue, Z., Hu, W., Liu, B., Liu, Y., Sun, X., Zhao, Q. and Di, K.: Quantitative analysis of the morphology of martian gullies and
600 insights into their formation, *Icarus*, 243, pp.208-221, doi: <https://doi.org/10.1016/j.icarus.2014.08.028>, 2014.

601